# Study on the Electronic Structures of the Reduced Anatase $TiO_2$ by the First-principles Calculations

*Zhijun Cheng, Tingyu Liu*, Chenxing Yang and Haixiu Gan*

College of Science, University of Shanghai for Science and Technology,

Shanghai 200093, P. R. China

*Feiwu Zhang*

Nanochemistry Research Institute, Curtin University, GPO Box U1987,

Perth, WA 6845, Australia

*Jianyu Chen*

Key Laboratory of Materials for High Power Laser, Shanghai Institute of Optics and Fine Mechanics，

Chinese Academy of Sciences, Shanghai 201800, PR China

**Abstract**

Employing the first-principles calculations based on the density functional theory (DFT) and the Molecule Orbital theory (MO), we have researched the electronic structures of the reduced anatase $TiO_2$ and its visible light photoactivity. The study is emphasized on the O vacancy, including the components of the defect states, the relationship with the bulk states and the way in which these electrons occupying the defect states are distributed in the real space. We find that the origin of the visible light photoactivity should be due to the transition of the excited electrons from the defect states $\sigma_g$ orbital to the $\sigma_u$ orbital in the upper conduction bands, rather than arising from the reduction of the band gap. The calculated

*Corresponding author. Email: liutyyxj@163.com Tel: 086-021-65667034

results indicate that the localized defect states induced by the neutral and doubly ionized oxygen vacancies are all located in the band gap.

**Keyword:** Oxides; Ab initio calculations; Defects; Electronic Structure

## 1. Introduction

Because of its unique advantages such as high oxidizing power and durability, anatase $TiO_2$ has been widely used as a semiconductor photocatalyst in the fields of purification of air and water[1-3], hydrogen production and so on. But due to its large band gap (3.2eV), $TiO_2$ cannot absorb the visible solar radiation (about 50% of the solar radiation energy), greatly lowering the catalytic efficiency and limiting its application ranges. Consequently, it has long been one of the key issues how to utilize the visible light and enhance the catalytic efficiency. People have developed many optimizing schemes such as coupling with other semiconductor photocatalysts, e.g., $WO_3$[4], $ZrO_2$[5], $In_2O_3$[6], to accelerate the charge separation in the photocarriers generation process, or doping metal/non-metal ions into $TiO_2$ so as to reduce the band gap and extend the photocatalytic activity into the visible spectrum[7]. But unfortunately some dopants may also play roles of carrier scattering centers and traps, which are unfavorable for the enhancement of catalytic efficiency. Therefore, it is essential to examine all of the aspects about the doping before completely mastering the enhancement mechanism.

The native defects can be easily formed under a variety of conditions[8] and it is not appropriate to ignore their effects on the catalytic process, resulting in difficulty to judge which one plays the key role in the improvement of the photocatalytic efficiency. Rumaiz et al.[9] recently examined the oxygen vacancies in the N-doped anatase $TiO_2$. They found that the N-doping would lead to the formation of the oxygen vacancies. The combination of nitrogen and oxygen vacancy was accounted for the observed visible-light catalytic behavior. Meanwhile, Lin et al.[10] presented their theoretical calculations on the electronic structures and absorption spectra of $TiO_2$ with substitutional N and O vacancy at different concentrations. It was found that the absorption below 500 nm was mainly due to the N states located above the valence bands, while absorption above 500 nm was mainly caused by O vacancies. On the

other hand, Justicia et al.[11] also demonstrated that the reduced forms of titania $TiO_x$ (x<2) in the anatase phase would act as an efficient photacatalyst. They pointed out that the neutral vacancy-induced electronic states just below the conduction band seemed to be responsible for the large photodegradation activity and the reduced $TiO_2$ could absorb the visible light as well. Other research groups[12,13] also produced visible-light active $TiO_2$ catalysts and found that it was the oxygen vacancy's donor states located below the conduction bands that gave rise to the visible-light photoactivity.

Although there have been plenty of studies on the O vacancies in anatase $TiO_2$, many features have not been precisely understood and even some apparent divergences occasionally exist. Na-Phattalung et al.[14] studied all of the possible native point defects in the anatase $TiO_2$ modeled by a 108-atom supercell. In their work, the O vacancy with +2 charge state had the lowest formation energy compared to that of the 0 or +1 charge state under any possible equilibrium growth conditions. The $V_O^{2+}$ induced the delocalized resonant electronic states with the Ti d character, not in the band gap but above the CBM (conduction band minimum). This result was identical to the case of $V_O^{2+}$ in the reference [11]. In contrast, Sullivan and Erwin[15] also researched the native defects by the first-principles method using a supercell consisting of 108 atoms. They presented that the thermodynamic transition levels[16] between the +2 and +1 as well as +1 and 0 charge states were all just below the CBM, implying that the $V_O^{2+}$ would induce the defect energy levels in the band gap. Even though the conclusions about the defect states of neutral $V_O$ [10,11,15] are basically consistent with each other, i.e., locating in the band gap about 0.1-0.3eV below the CBM mainly with Ti 3d character, the entire study on the O vacancy including the components of the defect states, the relationship with the bulk states and the way in which these electrons occupying the defect states are distributed in the real space, has not been found in any newly published literatures, as far as we know. In this paper, we will investigate the neutral and doubly ionized oxygen vacancies using the first-principles total-energy calculations to offer the theoretical background for developing the low-cost visible-light photocatalysts.

## 2. Computational methods

The first-principles calculations are based on the density functional theory (DFT) using the plane-wave pseudopotential[17,18] method implemented in the Vienna Ab-initio Simulation Package ( VASP ) codes[19]. The energy cutoff is chosen as 520 eV to avoid the Pulay stress[20] arising from the incompleteness of the plane wave basis set and the ultrasoft pseudopotentials[21] are used to present the valence configurations $3d^3 4s^1$ for Ti and $2s^2 2p^4$ for O. The local density approximation (LDA) for exchange-correlation functional is adopted.

The 0 (or +2) vacancy is modeled by taking out one oxygen atom (or oxygen ion with -2 charge state ) from the supercell containing 48 atoms built from the 2×2×1 repetition of the unit cell, a typical supercell size[22,23] for studying defect properties in rutile $TiO_2$. In the 48-atom rutile supercell, the shortest defect-defect distance is about 6 Å while the anatase phase's is about 7.5 Å. In order to check the effects of the supercell size and shape on the calculations, Na-Phattalung et al.[14] repeated a series of the calculations with different supercells and found that the formation energies of the native defects in the 48-atom supercell were acceptable compared to that in the 108-atoms one, typically within 0.45eV. The Monkhorst-Pack k-point sampling[24] is set as 3×3×3 for the supercell and 9×9×9 for the primitive cell, ensuring the change of the total energy within 0.01eV. The supercell is fully optimized with the supercell's shape and volume changeable until the forces acting on the ions are less than 0.01eV/Å.

The crystal structure parameters are obtained following the scheme described below. Firstly we obtain the equilibrium volume $V_0$ and bulk module $B_0$ by fitting the Murnaghan equation of states[25]:

$$E(V) = E_0 + \frac{B_0 \times V}{B_p} \times [\frac{(\frac{V_0}{V})^{B_p}}{B_p - 1} + 1] - \frac{V_0 \times B_0}{B_p - 1} \quad (1)$$

where E is the total lattice energy for the primitive cell in eV, V is the cell's volume in $Å^3$, $E_0$ is the binding energy in eV, $B_0$ is the bulk module in Gpa, and $B_p$ is defined as $B_p = (\frac{\partial B_0}{\partial P})_{V_0}$. For each cell's volume, the shape (c/a) and the coordinates of the ions are allowed to relax so as to minimize both the total energy and the forces acting on the ions. Secondly, by changing the total energy as a function of the lattice parameter a, with the cell's volume fixed at the equilibrium value, i.e., $V=V_0$, we may pick

out the equilibrium lattice parameters $a_0$ and $c_0$ which have minimized the energy and the forces as well. Finally, we relax the ions in the cell obtained previously to gain the optimal internal parameter u, defined as $u=d_c/c$ ($d_c$ is the Ti-O bond length paralleling to the c axis). During the calculations, the convergence criterion for the residual force is less than 0.01eV/Å. The optimized lattice parameters are listed in Table 1.

Due to the periodic boundary condition, there are fictitious electrostatic interactions between the charged defect and its images. Nevertheless, the Makov-Payne correction[26] is not employed due to the fact that the dielectric constant of $TiO_2$ is very large ($\epsilon$ >100) and hence leads to the main correction term $e^2q^2\alpha/L/\epsilon$ negligible (where q is the net charge of the defect, $\alpha$ is the Madelung constant and L is the distance between the defect and its image).

Lin et al.[10] presented the spin-polarized DFT calculations. Their results showed that the donor states induced by the neutral oxygen vacancies were occupied by almost equal numbers of spin-up and spin-down electrons. For this reason, we carry out our calculations with the spin restricted.

The formation energy[16] of the O vacancy in charge state +q is defined as:

$$E_f[V_o^{+q}] = E_{tot}[V_o^{+q}] - E_{tot}[bulk] + \mu_o + q\times[E_F + E_V + \Delta V] \qquad (2)$$

where $E_{tot}[V_o^{+q}]$ is the total energy of the supercell with one $V_o^{+q}$, $E_{tot}[bulk]$ is the total energy for the equivalent perfect supercell, $\mu_o$ is the chemical potential for the species of oxygen, $E_F$ is the fermi level with respect to the bulk valence-band maximum (VBM), $E_V$, and $\Delta V$ is a correction term to align the reference potential in the defect supercell with that in the perfect bulk. The discussion on the chemical potential and its boundary conditions can be found in the work by Na-Phattalung et al.[14]. Since the charged defects will induce a constant shift in the potential, we can evaluate $\Delta V$ by comparing the local electrostatic potential far away from the defect site in the cell with that in the perfect one.

Table 1

## 3. Results and discussion

### 3.1. Stoichiometric $TiO_2$.

$TiO_2$ in anatase phase possesses the space group of I41/AMD (No. 141) with a body centered tetragonal lattice. The space lattice is formed by the addition of the atomic basis, which consists of two formulae, to every lattice point of the body centered tetragonal lattice. As a result, each unit cell owns two atomic bases, i.e., four $TiO_2$ formula units. Each Ti ion is coordinated to the six nearest-neighboring O ions forming distorted $TiO_6$ octahedra with two kinds of bonds, two apical (paralleling to the c axis, $d_{ap}$) and four equatorial bonds ($d_{eq}$). Meanwhile, each O ion is coordinated to three Ti ions in a plane through two equatorial bonds and one apical bond, forming the $Ti_3O$ cluster. The distorted $TiO_6$ octahedra shares the four edges and four vertexes with each other.

The structure of anatase, as shown in Fig. 1 (a), can be described in terms of a, c and the internal parameter u, defined as $u=d_{ap}/c$. In table 1, we have listed the optimized structure parameters compared with both the experimental values[27] reported below 1000 K, and the previous theoretical ones[28] using the full-potential linearized augmented plane-wave (FLAPW) scheme[29]. Our results agree well with those of the experiment measurements and the previous simulations[14,29].

Fig. 1 (a), (b) and (c)

Noteworthily, our simulation approaches acquire a better improvement in the bulk module ($B_0$) than the previous theoretical result[31] with $B_0$ (175 GPa) only underestimating the experiment's result[30] (179 GPa) by 2.2%.

The electronic band structure and the related Density of the States (DOS) around the Fermi level for the perfect 48-atom supercell along the high symmetry directions are depicted in Fig. 2(1) and (2). The Fermi level (the top of the valence band) is set as the reference energy. A minimal direct band gap, about 2.0eV, can be found at G (the center of the brillouin zone), the same value as the FLAPW calculation's[28]. Because the periodic boundary conditions in the 48-atom supercell are different from

those in the unit cell, one should note that the Bravais lattice will transform from the body centered tetragonal for the unit cell to the simple tetragonal for the 48-atom supercell. Correspondingly, the first brillouin zone is also different for each case.

Figure 2

We have also calculated the band structure of the unit cell, obtaining an indirect minimal band gap from X to G but with the same band gap magnitude. This may be the reason for the difference between the works of Asahi et al. and Lin et al. The calculated band gap (2.0 eV) is much smaller than the experimental result (3.2 eV) due to the well-known shortcoming of LDA.

**3.2. Double ionized oxygen vacancy.**

After the defect supercell is optimized, the total energy is about 2.7 eV lower than the initial value. Along with the volume of the supercell compressed by about 2.6%, the three Ti ions in the $Ti_3V_o$ cluster are displaced by 0.1-0.3 Å outward from the vacancy site and oppositely the neighbouring O ions are shift inward by 0.15-0.22 Å. This is caused by the effective positive charges of the vacancy that interact repulsively with the cations and attractively with the anions. To investigate the change of the electrons distribution, we have also calculated the effective charges on the ions according to the Bader (topological) analysis[32].

Figure 3

The Ti (O) ion in the bulk possesses about 1.5 e (7.2e). As to the current case, the Bader effective charges on the ions have reduced slightly, especially for those which have offered the defect states to the vacancy. For example, comparing with the related values in the supercell with a neutral oxygen

vacancy as described in the following section, each of the three Ti ions in the $Ti_3V_o$ cluster has reduced about 0.13-0.08 e and the nearest two O ions also cut about 0.07 e down respectively while the others are less than 0.05 e. The results indicate that these two additional electrons for the neutral vacancy are mainly distributed among the ions nearby the vacancy site and hence should occupy certain electronic states of those ions. Indeed, this can be seen clearly from the band structures in Fig.2, the density of states in Fig. 3, and the charge density distributions in Fig. 4.

In Fig. 2(5) (corresponding to the $V_O^{2+}$), the relatively flat defect states indicated by an arrow are about 0.4 eV in average below the conduction band edge with a width of 0.5 eV. The weak dispersion is caused by the illusory interactions between the charged defect and its images in the finite supercell under the boundary conditions, which is also a common error in the DFT charged defects calculations using the supercell approach. For comparison, we calculate another equivalent supercell also containing a +2 oxygen vacancy but without optimizing the structure. By analyzing its electronic structure, we find that the defect states are much deeper than the relaxed case and don't overlap with the extension states of the conduction band. So the shift of the localized defect levels should be attributed to the relaxation of the nearby ions, i.e., the effective potential well is reduced after relaxation and then it is not strong enough to trap the electrons locally. This can be further confirmed from the total local potential analysis in Fig. 5 presented later.

In Fig. 3, we show the total electron density of states (TDOS) of $V_O^{2+}$ in (1) and the site decomposed local partial density of states (LPDOS) of Ti and O in (2) and (9) respectively. The remaining plots are the angular-momentum components of the local partial density of states (LPDOS). It should be noted that, as depicted in Fig. 1, the $Ti_3V_o$ cluster is in the xoz plane. The Ti in Fig. 3 refers to one of the three Ti ions in the $Ti_3V_o$ cluster and O is one of the two oxygen ions nearest neighboring to the vacancy. We also checked the partial density of states (PDOS) of other Ti and O in the $Ti_3V_o$ cluster and found that the results were almost unchanged. Just as pointed by Asahi et al.[28], region (I) in Fig. 3 is due to the $\sigma$ bonding ($\sigma_g$) arising from the hybridization of the O $p_\sigma$ ($p_x$ and $p_z$ in the $Ti_3V_o$ cluster plane) and Ti $e_g$ ($d_{x^2}$, $d_{z^2}$) orbital, region (II) is due to the $\pi$ bonding ($\pi_u$) from the hybridization of the O $p_\pi$ ($p_y$)

and Ti $d_{xz}$ (or $d_{yz}$), region (V) and (IV) are due to $\pi$ antibonding ($\pi_g$) and $\sigma$ antibonding ($\sigma_u$) respectively. The top of the valence band is mainly resulted from the O $p_\pi$ ($p_y$) which is non-bonding and the bottom of the conduction band consists of the isolated Ti $d_{xy}$ orbital. Nonetheless, different from other group's results[14], we find that the defect states related to the $V_O^{2+}$, as plotted in region (III), are in the band gap just under the conduction band edge. From region (III), it can be concluded that the defect states are mainly composed of Ti 3d, which is the same as the results of other groups. But as a matter of fact, the defect states also contain such significant components as Ti $s$, Ti $e_g$, Ti $t_{2g}$ (only $d_{xz}$) and especially the O $p_\sigma$, and it is not reasonable to ignore their contributions. The absence of Ti $d_{yz}$, Ti $d_{xy}$ and O $p_\pi$ ($p_y$) orbitals indicates that the defect states are mainly distributed in the $Ti_3V_o$ plane (i.e., the xoz plane in the current case), which can be verified by Fig. 4 (b) and (c). The charge densities of the defect states at Z are presented in Fig. 4 to illustrate the detailed electronic structure features of the $V_O^{2+}$.

Figure 4 (a), (b) and (c)

From Fig.4 (a), we can see that these two additional holes are not totally bounded around the vacancy site but also occupy the $\sigma_g$ orbital between Ti and O ions, which is actually very important for the oxygen vacancy to play a role in the photocatalyzed processes and we will give a detailed discussion in the next section.

Finally, we also investigate the thermodynamic transition level between the +2 and 0 vacancies, $\epsilon$ (+2/0). The thermodynamic transition level $\epsilon$ (+2/0) is defined as the Fermi-level position where the +2 and 0 vacancies have equal formation energy. Before this can be done, we calculate the averaged total local electrostatic potential energies along different directions, as presented in Fig. 5.

Figure 5

The five minima along a and c axes respectively in Fig. 5 are directly related to the five atom layers in the three supercells, one of which the vacancy is located in is marked with an arrow. It may be acquired from Fig. 5 that the local potential at the place far away from the defect site in the supercell with $V_O^{2+}$ is lowered about 0.2 eV, comparing with that of the perfect one in the same sites both along a and c axes. So we can set the value of $\Delta V$ in equation (2) as 0.2 eV to align the electrostatic potential in the perfect bulk. Besides, $E_V$ is evaluated as the difference between the total energy of a perfect supercell and that of the same supercell with one electron removed from the VBM. According to our calculations, $E_{tot}[V_o^0]$ = -457.996 eV, $E_{tot}[bulk]$ = -468.692 eV, $E_{tot}[V_o^{+2}]$ = -466.812 eV and $E_V$ = 2.09 eV. So following the definition of the thermodynamic transition level, we have $E_f[V_o^{+2}] = E_f[V_o^0]$ and, as a result of this, the thermodynamic transition level $\epsilon(+2/0)$ is 2.1 eV.

Figure 6

**3.3. Neutral oxygen vacancy.**

The total energy of the relaxed supercell with one $V_O^0$ is lowered about 0.4 eV from the initial state, which is much smaller than that of the double ionized one. This little energy change is due to the fact that the electric equilibrium is still remained after we picked out an oxygen atom from the perfect supercell. Furthermore, since the atomic radius of oxygen (0.66 Å) is less than half of the titanium's (1.47 Å), the stress caused by the missing of the O atom is slight too. The ions around the oxygen vacancy behave similarly to those in the $V_O^{2+}$ case arising from the effective charges of the vacancy site too, but are disparted closer by about 0.04 Å.

Comparing with the bulk's values, we find that the effective charge on each of the three nearest Ti increases by 0.12-0.16e, accompanying a comparable augment on both of the nearest two O by about

0.09e. The charge changes on other ions are typically less than 0.01e. Again, these results indicate that the two additional electrons are mainly distributed among the ions nearby the vacancy site.

Not surprisingly, the band structure for the $V_O^0$ in Fig 2 (3) and the DOS plots in Fig. 6 are quite similar to those of the $V_O^{2+}$ and thus we propose that the defect states of the oxygen vacancy are independent of its charge states. So, for conciseness, we will not discuss the detailed electronic structures for the $V_O^0$ any longer.

Based on the calculated electronic structure of the neutral oxygen vacancy, the enhanced visible light photoactivity of the reduced titania $TiO_x$ (x<2) may be understood easily. According to the molecule orbital theory (MO), the electronic transition between u and u (or g and g) is forbidden by the selection rules, which instead allows the electrons to hop between the u and g orbitals. As a result, the excited electrons occupying the defect states $\sigma_g$ orbitals in region (III) will first jump to the $\sigma_u$ orbitals in region (IV) in the upper conduction bands and finally get back to the $\pi_g$ orbitals in region (V). At last，these free charge carriers will move to the surface and take part in the processes of photocatalytic reactions. Furthermore, the excited electrons in the conduction band will not recombine with the holes in the defect states, again restrained by the selection rules.

Although the band gap is not correctly produced by the LDA calculations, yet the depth of these donor levels (relative to the conduction edge) is essentially independent of the value of the computed band gap[14,15]. The precise energy ranges of region (III) and (V) are (-0.24, 0.32) and (2.77, 5.07) respectively and thus the minimum energy to excite the electrons is 2.45 eV, corresponding to 507 nm. That's exactly what have been observed in the related optical absorption and photocatalytic experiments[9,11]: the absorption tail for the titania with oxygen sub-stoichiometry is close to 500 nm and could present enhanced photocatalytic properties in the visible light range. On the other hand, the minimum band gap for the supercell with a $V_O^0$ in our calculations is about 0.2 eV larger than the perfect one's, which further convinces us that the enhancement of the visible light photocatalytic properties should not be attributed to the reduction of the band gap.

**4. Conclusion**

To sum up, we have presented that the electronic structures arising from the oxygen vacancy are independent of the charge states. Combining the calculated electronic structures and the molecular obitals theory, we demonstrated theoretically that the reduced $TiO_2$ could be an efficient visible light photocatalyst up to 507 nm, consisting very well with the relevant experiments. Detailed processes about the light-catalyzed reactions will be studied in our further work.

**Acknowledgment**

This work is supported by the Innovation Fund Project for Graduate Student of Shanghai (JWCXSL1002), the Foundation of Shanghai Municipal Education Committee (Grant No. 09YZ210) and the Shanghai Leading Academic Discipline Project (S30502). The authors would like to express their grateful appreciation to Prof. Zhang Qiren for his helpful discussions.

**References**

(1) Gogate, P. R.; Pandit, A. B. Adv. Environ. Res. 2004, 8, 501-551.

(2) Gaya, U. I.; Abdullah, A. H. J. Photoch. Photobio. C: Photochem. Rev. 2008, 9, 1-12.

(3) Bhatkhande, D. S.; Pangarkar, V. G.; Beenackers, A. C. M. J. Chem. Technol. Biotechnol. 2001, 77, 102-116.

(4) Engweiler, J.; Harf, J.; Baiker, A. J. Catal. 1996, 159, 259-269.

(5) S. P., Fen; G. W. Meng; L. D. Zhang Chin. Sci. Bull. 1998, 43, 1613.

(6) Poznyak, S. K; Talapin, D. V.; Kulak, A. l. J. Phys. Chem. B 2001, 105, 4816-4823.

(7) Ni, M.; Leung, M. K. H; Leung, D. Y. C; Sumathy, K. Renew. Sust. Energ. Rev. 2007, 11, 401-425.

(8) He, J.; Behera, R.K.; Finnis, M.W.; Li, X.; Dickey, E.C.; Phillpot, S.R.; Sinnott, S.B. Acta Materialia 2007, 55, 4325-4337.

(9) Rumaiz, A. K.; Woicik, J. C.; Cockayne, E.; Lin, H. Y.; Jaffari, G. H.; Shah, S. I. Appl. Phys. Lett. 2009, 95, 262111-262111-3.

(10) Zheshuai, Lin; Alexander, Orlov.; R. M. Lambert.; M. C, Payne. J. Phy. Chem. B 2005, 109, 20948-20952.

(11) Justicia, I.; Ordejon, P.; Canto, G.; Mozos, J. L.; Fraxedas, J.; Battiston, G. A.; Gerbasi, R.; Figueras, A. Adv. Mater. 2002, 14, 1399-1402.

(12) Ihara, T.; Ando, M.; Sugihara, S. Photocatalysis 2001, 5, 19-22.

(13) Ihara, T.; Miyoshi, M.; Iriyama, Y.; Matsumoto, O.; Sugihara, S. Appl. Catal. B 2003, 42, 403-409.

(14) Na-Phattalung, S.; Smith, M. F.; Kim, K.; Du, M. H.; Wei, S. H.; Zhang, S. B.; Limpijumnong, S. Phy. Rev. B 2006, 73, 125205.

(15) Sullivan, J. M.; Erwin, S. C.; Phy. Rev. B 2003, 67, 144415.

(16) Van de Walle, C. G.; Neugebauer, J. J. Appl. Phys. 2004, 95, 3851-3879.

(17) Payne, M. C.; Teter, M. P.; Allan, D. C.; Arias, T. A.; Joannopoulos, J. D. Rev. Mod. Phys. 1992, 64, 1045-1097.

(18) Segall, M. D.; Lindan, P. J. D.; Probert, M. I. J.; Pickard, C. J.; Hasnip, P. J.; Clark, S. J.; Payne, M. C. J. Phys. : Condens. Matter 2002, 14, 2717-2744.

(19) Kresse, G.; Furthmüller, J. Comput. Mater. Sci. 1996, 6, 15.

(20) Francis, G P; Rayne, M C J. Phys.: Condens. Matter 1990, 2, 4395-4404.

(21) Vanderbilt, D. Phys. Rev. B 1990, 41, R7892.

(22) Ramamoorthy, M.; King-Smith, R. D.; Vanderbilt, D. Phys. Rev. B 1994, 49, 7709.

(23) Lindan, P. J. D.; Harrison, N. M.; Gillan, M. J.; White, J. A. Phy. Rev. B 1997, 55, 15919.

(24) Monkhorst, H. J.; Pack, J. D. Phys. Rev. B 1976, 13, 5188-5192.

(25) Murnaghan, F. D. Proc. Natl. Acad, Sci. 1944, 30, 244.

(26) Makov, G.; Payne, M. C. Phy. Rev. B 1995, 51, 4014.

(27) Horn, M.; Schwerdtfeger, C. F.; Meagher, E. P. Z. Kristallogr. 1972, 136, 273–281.

(28) Asahi, R.; Taga, Y.; Mannstadt, W.; Freeman, A. J. Phy. Rev. B 2000, 61, 7459.

(29) Wimmer, E.; Krakauer, H.; Weinert, M.; Freeman, A. J. Phys. Rev. B 1981, 24, 864.

(30) Arlt, T.; Bermejo, M.; Blanco, M. A.; Gerward, L.; Jiang, J. Z.; Olsen, J. S.; Recio, J. M. Phys. Rev. B 2000, 61, 14414.

(31) Rubio-Ponce, A.; Conde-Callardo, A.; Olguin, D. Phys. Rev. B 2008, 78, 035107.

(32) Henkelman, G.; Arnaldsson, A.; Jonsson, H. Commput. Mater. Sci. 2006, 36, 354.

## Figure captions

Figure 1 The optimized atomic structures for: (a) bulk anatase, (b) neutral oxygen vacancy, (c) double ionized oxygen vacancy. The large gray spheres are the Ti atoms and the small black ones are the O atoms. The definitions of the coordinates and the apical ($d_{ap}$) and equatorial ($d_{eq}$) bond length along with their angle ($2\theta$) are indicated in (a) as well. The $Ti_3V_o$ cluster is also shown in (b).

Figure 2 The band structures and related density of states around the Fermi level for: bulk (1 and 2), neutral vacancy (3 and 4) and double ionized vacancy (5 and 6). The Fermi levels are indicated by the horizontal dot lines and the energy bands related to the defects are marked with small arrows.

Figure 3 The different theoretical density of states for the Ti, one of the three Ti ions in the $Ti_3V_o$ cluster, and O, which is nearest to the defect site in the supercell containing a $V_O^{2+}$. Multipliers relative to the O $P_z$ component are indicated in each case. The vertical dot lines are plotted to distinguish different regions of the electronic structures.

Figure 4 The densities of the holes occupying the defect states at Z point for the supercell with a $V_O^{2+}$ in the (010), (100) and (001) planes, all of which pass through the vacancy site, are plotted in (a), (b) and (c) respectively. The positions of the atoms and the vacancy in the planes are indicated. The contours start from $4\times10^{-3}$ holes/a.u.$^3$ and the interval is 0.004.

Figure 5 The averaged total local electrostatic potential energy in a and c directions. The sampling points along certain direction within the range of the supercell are set as the horizontal axis. The local electrostatic potential in the plane which passes through a sampling point but perpendicular to the specific direction is averaged. The insets present the detailed local potential at the place away from the defect site in the supercell.

Figure 6 The density of states for the supercell with one neutral oxygen vacancy. The detailed description can be found in the captions for Fig. 3.

Table

TABLE 1: The structure properties for anatase $TiO_2$ compared with that of the experimental and theoretical results respectively. The difference between the calculated and measured value is shown as a percentage in parenthese.

| | Exp.[27] | This work | FLAPW[28] |
|---|---|---|---|
| a (Å) | 3.784 | 3.764(-0.5%) | 3.692(-2.4%) |
| c (Å) | 9.515 | 9.461(-0.6%) | 9.471(-0.5%) |
| $d_{eq}$ (Å) | 1.934 | 1.923(-0.6%) | 1.893(-2.1%) |
| $d_{ap}$ (Å) | 1.980 | 1.972(-0.4%) | 1.948(-1.6%) |
| c/a | 2.514 | 2.514(0.0%) | 2.566(+2.1%) |
| u | 0.208 | 0.208(0.0%) | 0.206(-1.0%) |
| 2θ | $156.2^o$ | $156.4^o$ (+0.1%) | $154.4^o$ (-1.2%) |
| $V_0(Å^3/TiO_2)$ | 34.06 | 33.52(-1.2%) | 32.27(-5.3%) |

**Figures**

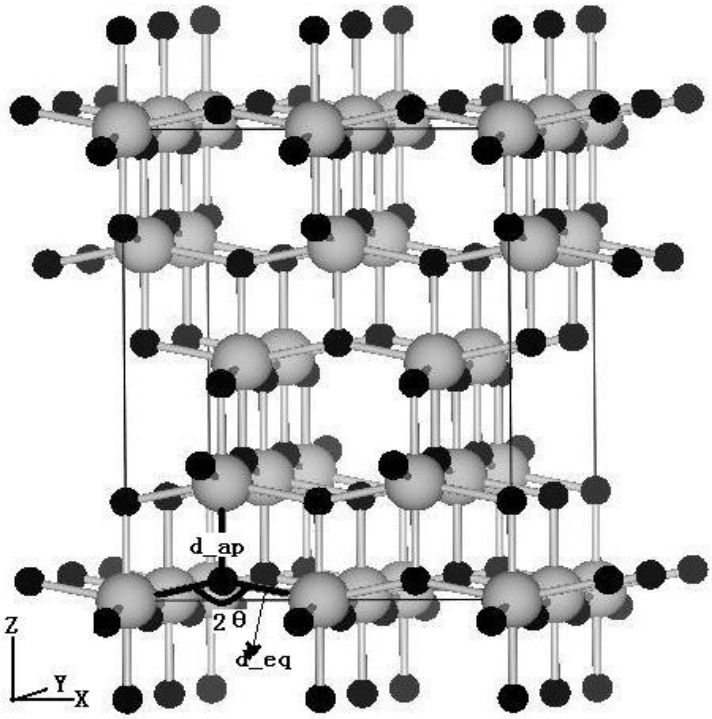


Fig 1 (a)

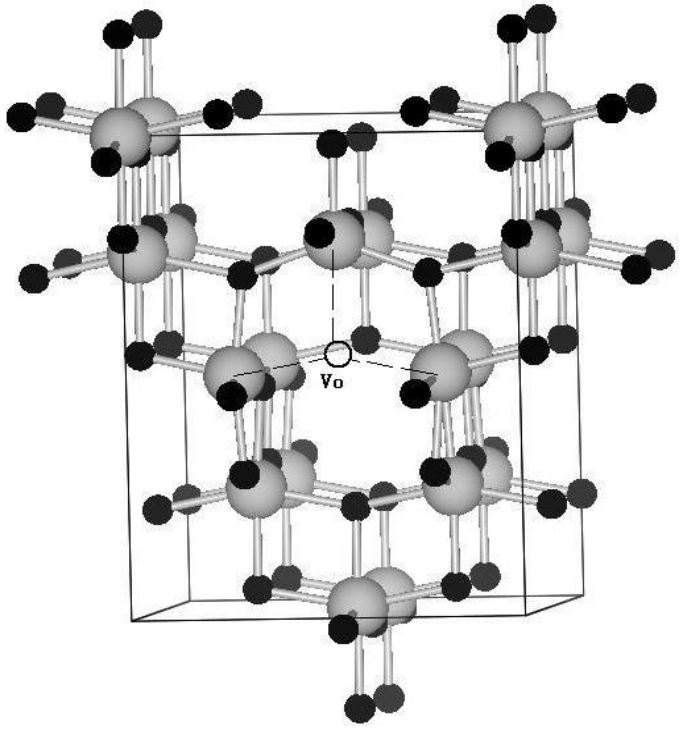


Fig 1 (b)

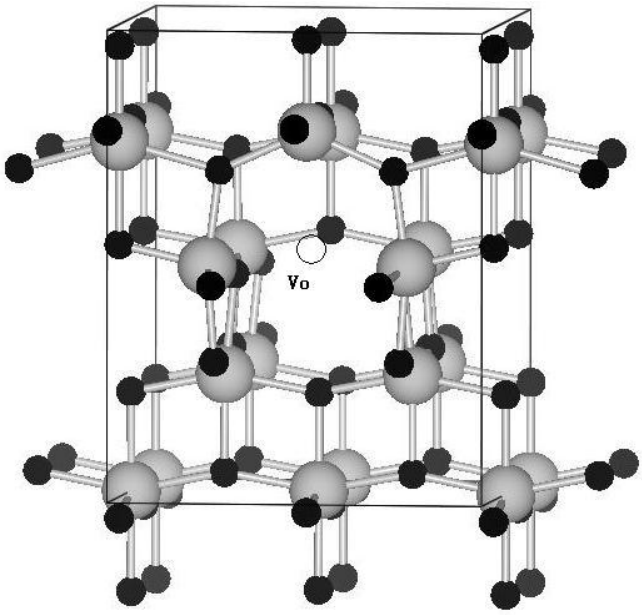


Fig 1(c)

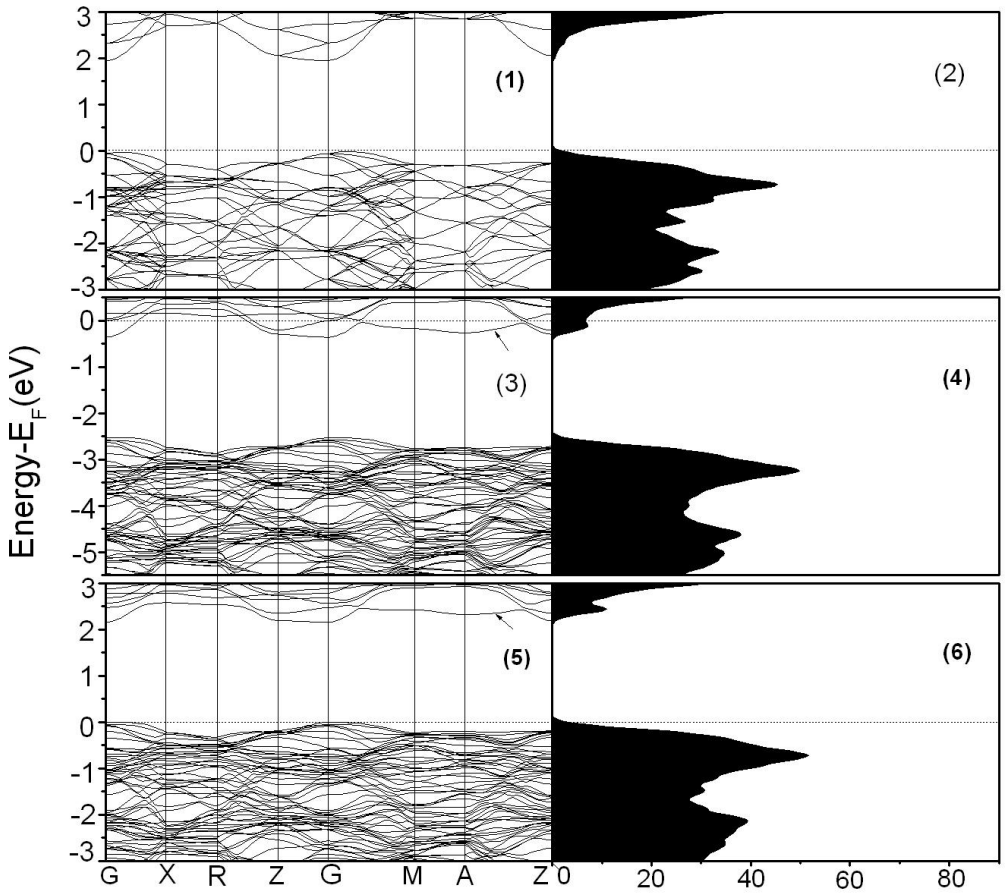


Fig 2

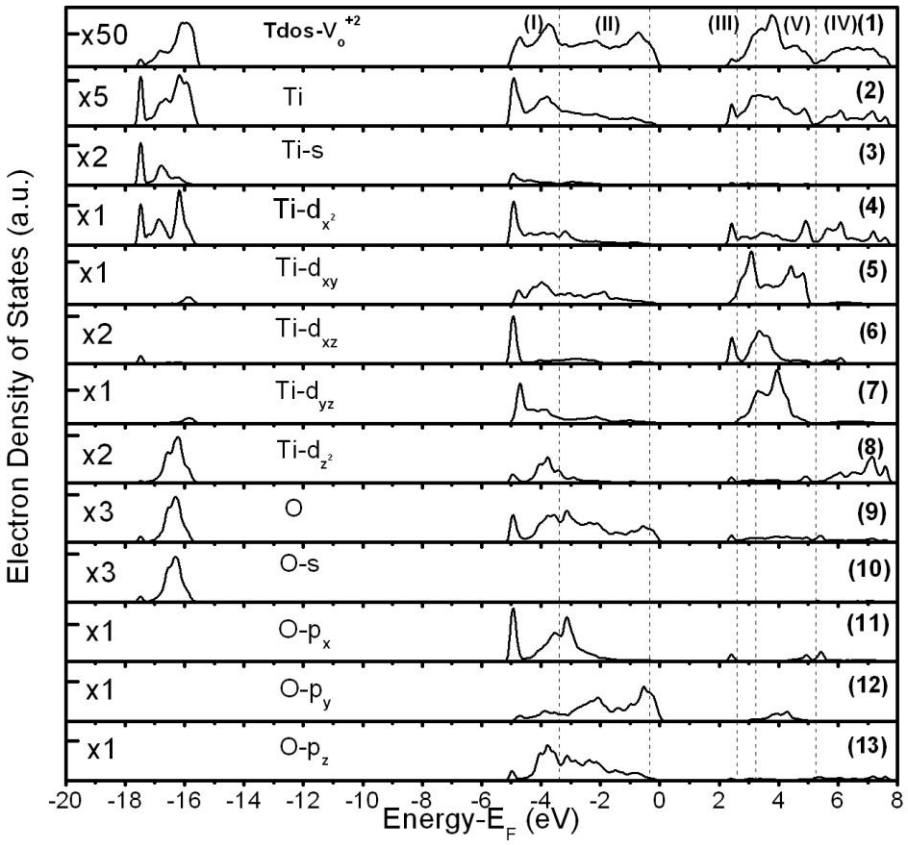
Electron Density of States (a.u.)
x50
Tdos-V$_o^{+2}$
(I)
(II)
(III)
(V)
(IV)
(1)
x5
Ti
(2)
x2
Ti-s
(3)
x1
Ti-d$_{x^2}$
(4)
x1
Ti-d$_{xy}$
(5)
x2
Ti-d$_{xz}$
(6)
x1
Ti-d$_{yz}$
(7)
x2
Ti-d$_{z^2}$
(8)
x3
O
(9)
x3
O-s
(10)
x1
O-p$_x$
(11)
x1
O-p$_y$
(12)
x1
O-p$_z$
(13)
-20 -18 -16 -14 -12 -10 -8 -6 -4 -2 0 2 4 6 8
Energy-E$_F$ (eV)

Fig 3

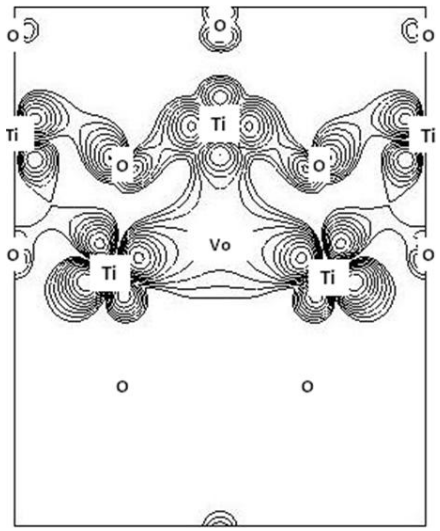
O
Ti
Ti
O
O
Vo
Ti
Ti
O
O

Fig 4 (a)

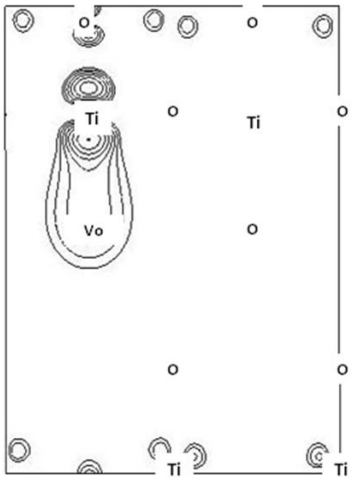


Fig 4 (b)

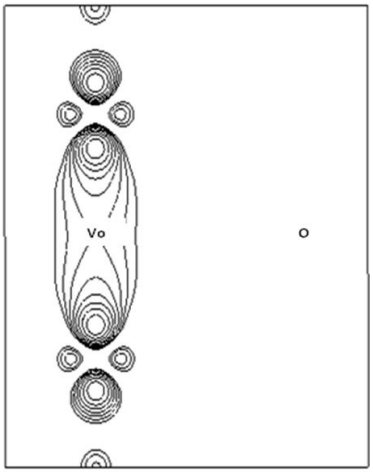


Fig 4 (c)

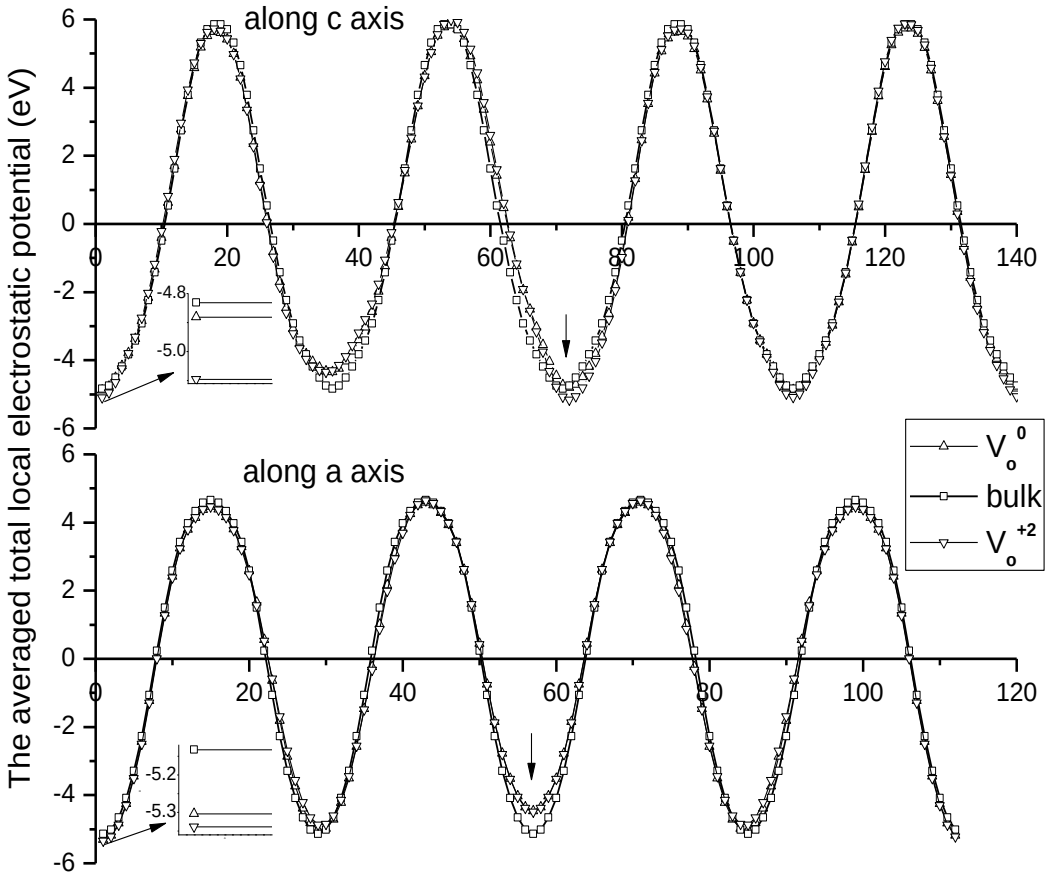
along c axis
along a axis
The averaged total local electrostatic potential (eV)
$V_o^0$
bulk
$V_o^{+2}$

Fig 5

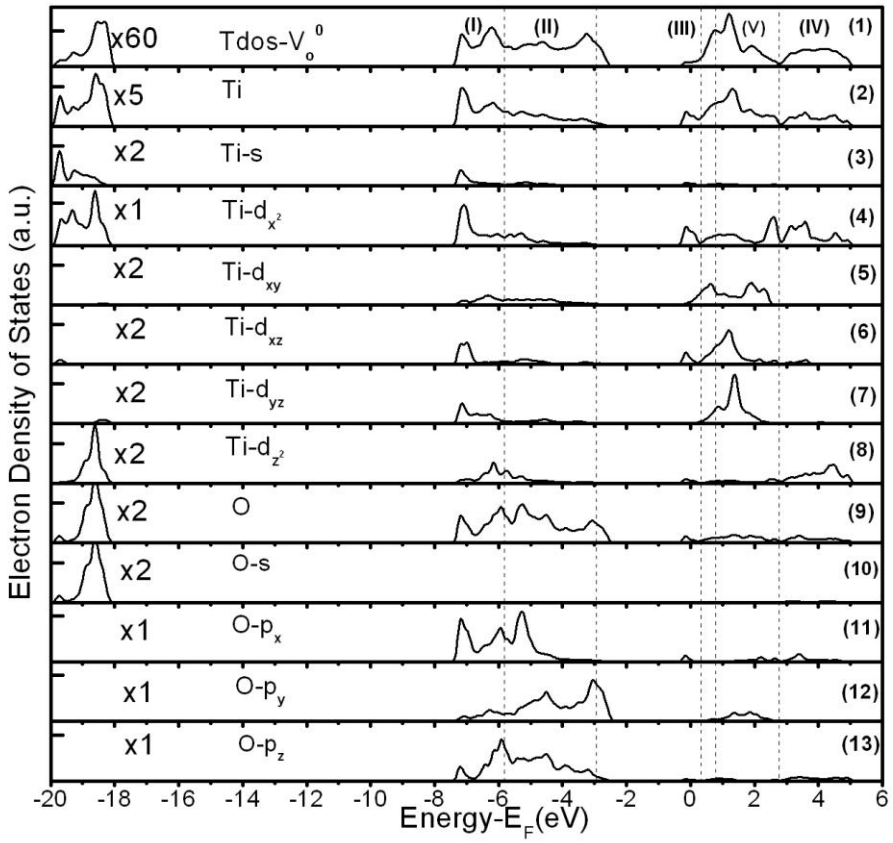
Tdos-$V_o^0$
Ti
Ti-s
Ti-$d_{x^2}$
Ti-$d_{xy}$
Ti-$d_{xz}$
Ti-$d_{yz}$
Ti-$d_{z^2}$
O
O-s
O-$p_x$
O-$p_y$
O-$p_z$
Electron Density of States (a.u.)
Energy-$E_F$(eV)

Fig 6